

Alma Mater Studiorum Università di Bologna
Archivio istituzionale della ricerca

Effect of Photocrosslinking of D-A Thiophene Copolymers on the Performance of Single-Material Solar Cells

This is the final peer-reviewed author's accepted manuscript (postprint) of the following publication:

Published Version:

Lanzi, M., Salatelli, E., Marinelli, M., Pierini, F. (2020). Effect of Photocrosslinking of D-A Thiophene Copolymers on the Performance of Single-Material Solar Cells. *MACROMOLECULAR CHEMISTRY AND PHYSICS*, 221(2), 1-12 [10.1002/macp.201900433].

Availability:

This version is available at: <https://hdl.handle.net/11585/713336> since: 2023-05-05

Published:

DOI: <http://doi.org/10.1002/macp.201900433>

Terms of use:

Some rights reserved. The terms and conditions for the reuse of this version of the manuscript are specified in the publishing policy. For all terms of use and more information see the publisher's website.

This item was downloaded from IRIS Università di Bologna (<https://cris.unibo.it/>).
When citing, please refer to the published version.

(Article begins on next page)

This is the final peer-reviewed accepted manuscript of:

Massimiliano Lanzi, Elisabetta Salatelli, Martina Marinelli, Filippo Pierini, Effect of photocrosslinking of D-A thiophene copolymers on the performance of singlematerial solar cells, Macromol. Chem. Phys. 2020, 221, 1900433.

The final published version is available online at:
<https://doi.org/10.1002/macp.201900433>

Terms of use:

Some rights reserved. The terms and conditions for the reuse of this version of the manuscript are specified in the publishing policy. For all terms of use and more information see the publisher's website.

This item was downloaded from IRIS Università di Bologna (<https://cris.unibo.it/>)

When citing, please refer to the published version.

Effect of photocrosslinking of D-A thiophene copolymers on the performance of single-material solar cells

Massimiliano Lanzi ^{a,*}, Elisabetta Salatelli ^a, Martina Marinelli ^a, Filippo Pierini ^b

^a *Department of Industrial Chemistry “Toso Montanari”, University of Bologna, Viale Risorgimento 4, 40136 Bologna, Italy*

^b *Department of Biosystems and Soft Matter, Institute of Fundamental Technological Research, Polish Academy of Sciences, ul. Pawinskiego 5B, 02-106 Warsaw, Poland*

*Corresponding author. E-mail address: massimiliano.lanzi@unibo.it (M. Lanzi)

ABSTRACT

Side-chain C₆₀-fullerene functionalized alkylthiophene copolymers with different regioregularity and fullerene content have successfully been synthesized using a simple and straightforward post-polymerization functionalization procedure based on a Grignard-coupling reaction. The products have been employed as single materials in photoactive layers of organic photovoltaic (OPV) solar cells. The use of double-cable polymers has allowed an enhanced control on the nanomorphology of the active blend, reducing the phase-segregation phenomena as well as the macroscale separation between the electron acceptor and donor components. With the insertion of a thin layer of gold nanoparticles between buffer and active layer of the cells a conversion efficiency of 5.68% was obtained. Moreover, an increased stability over time was achieved when the copolymers were photocrosslinked immediately after the annealing procedure, leading to acceptable efficiencies even after 80 h of accelerated ageing, a key-feature for widespread applicability of the prepared devices.

HIGHLIGHTS

- First time reports the preparation of photocrosslinkable double-cable copolymers.
- Facile synthesis by post-polymerization functionalization.
- Reduced macroscale separation between ED and EA components.
- High photoconversion efficiency when a AuNPs layer is inserted.
- Long over time stability of OPV single-material cells.

Keywords: polythiophene; organic solar cells; thermal stability; photocrosslinking.

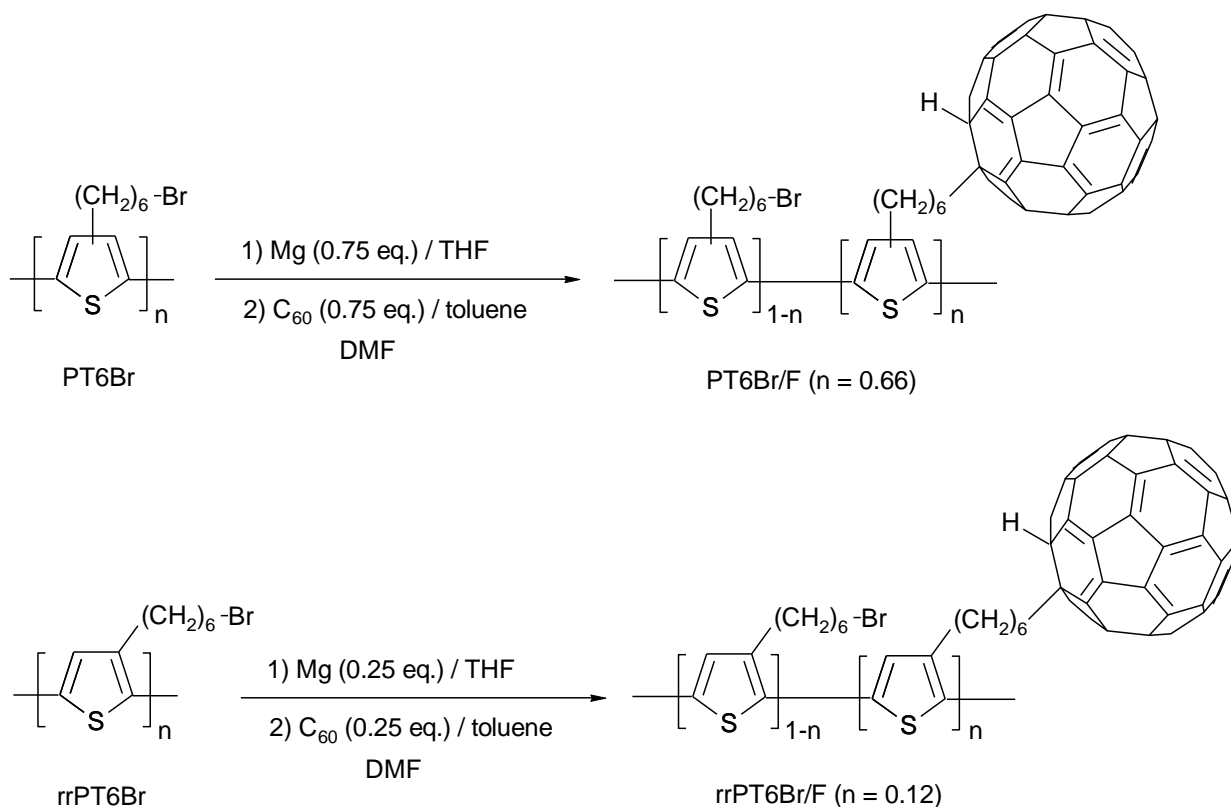
1. Introduction

Conjugated polymer-based organic photovoltaics have been intensively studied in the past decade owing to light-weight, flexibility and potential low-cost of polymer solar cells [1]. A significant improvement was obtained with the advent of bulk-heterojunction (BHJ) cells in which the structure provides a large interface area among the components of heterojunction (usually a blend of a conjugated polymer as electron-donor and a fullerene derivative as electron acceptor) thus facilitating the efficient generation of free charge carriers and their subsequent fast transport to the respective electrode [2]. Between the main layers, some other secondary (buffer) layers can be added in order to facilitate the charges migration and the conductance of electrodes [3]. However, it is difficult to obtain an optimized three-dimensional nanomorphology of the photoactive blend since the electron-donor (ED) and electron-acceptor (EA) components spontaneously tend to segregate. In fact, the ED-EA blend morphology arises from the kinetically freezing of a non-equilibrium state during the deposition process on the final substrate. The reduced miscibility of the two components often leads to the formation of fullerene clusters within the conjugated polymer matrix; since the positive carriers produced after the photoinduced charge separations are transported by the polymer and the electrons by the fullerene domains, the phase separation creates some “voids” which hinder

the charge transport through the electrodes. In polymer/fullerene blends, upon photoexcitation, an ultrafast forward electron-transfer reaction occurs ($t < 1\text{ps}$) [4] but the recombination of the photogenerated excitons in the blend is notably slower (some ms) being limited by the resonance stabilization due to the overlap of the electron and hole wave functions. During this time, however, the charges need to be carried effectively to the electrodes, and the random nature of the interpenetrating ED/EA network spontaneously formed during the deposition of the blend is undoubtedly an efficiency-limiting factor [5,6]. In order to prepare optimized phase-separated structures, some techniques have been recently proposed, such as the use of additives [7], compatibilizers [8], the covalent linkage of the EA molecules as pendants in the side-chain of the donor polymer [9-14] and the insertion of the acceptor group in the polymer main chain [15]. Anyhow, the efficiency of the devices using the fullerene in the side or main chain is strongly related to the EA content, which should be above the percolation threshold for the creation of a quasi-continuous donor network. It is then important to synthesize the ED/EA double-cable polymer with the appropriate fullerene content preserving, at the same time, an adequate solubility of the final material in common organic solvents. Moreover, most BHJ polymer solar cells show low thermal stability, since the photoactive blend spontaneously tends to give a macrophase separation in the micrometer scale [16] when exposed to heat during the annealing procedure or the exposition to the solar irradiation when tested in the solar cell device. This is mainly determined by the relatively low T_g of the polymers and the immiscibility of the components in the active layer. This disadvantage can be effectively prevented by inserting photocrosslinkable moieties in the conjugated polymer side-chains, as they can stabilize the BHJ film morphology without affecting the chain-packing, the number and dimension of EA domains and then the final efficiency of the photovoltaic cell [17].

In this paper, we report on the synthesis of some new thiophenic copolymers bearing both a C_{60} -fullerene moiety and a photocrosslinkable bromine group at the end of a hexamethylenic side chain.

The proposed structure is particularly intriguing and chemically elegant, as a single polymeric chain possess the ability to carry both the electrons and the positive holes (double-cable polymer). Moreover, this chemical structure can provide faster inter- and intra-chain transport of holes, a more effective displacement of the electrons along the fullerenes and a higher interfacial area between the donor and the acceptor, given that the segregation phenomena are strongly limited. The fullerene-substituted copolymers have been obtained using the postpolymerization approach, which has been demonstrated to facilitate the synthetic procedures required for the obtainment of polymers with the desired functional groups [18]. The two homopolymeric precursors were synthesized using two different polymerization methods, leading to two samples with similar molecular weights but different regioregularity degrees (PT6Br and rrPT6Br, Scheme 1). They were then functionalized with different amounts of fullerene to give PT6Br/F and rrPT6Br/F, respectively.



Scheme 1. Synthesis of PT6Br/F and rrPT6Br/F

The copolymers have been carefully characterized by means of chemical and spectroscopic techniques, the molecular arrangement of their films by atomic force microscopy (AFM) measurements and the effects of the regioregularity and fullerene content on the power conversion efficiency when employed as photoactive single materials in solar cells have been examined. Moreover, a thin layer of Au nanoparticles has also been tested as anode interlayer, giving a remarkable PCE of 5.68% with the best performing device, and the stability over time of the photocrosslinked cells compared with the uncrosslinked counterparts.

2. Experimental

2.1. Materials

All reagents were purchased from Sigma-Aldrich (Merck KGaA, Darmstadt, Germany). and used without further purification where not expressly indicated otherwise. All solvents used (HPLC grade) were dried and purified by normal laboratory procedures, stored over molecular sieves and handled in a moisture-free atmosphere.

2.2. Measurements

^1H - and ^{13}C -NMR were recorded on a Varian Mercury Plus (400 MHz) spectrometer using TMS as a reference. IR spectra were taken on Ge or KBr disks using a Perkin Elmer Spectrum One or a Bruker Alpha Platinum spectrophotometer. UV-Vis spectra were recorded on a Perkin Elmer Lambda 19 spectrophotometer using about 10^{-5} M polymer solutions in spectroquality solvents in Suprasil quartz cuvettes (1 cm \times 1 cm) or films on quartz slides. Molecular weights were determined by gel permeation chromatography (GPC) by using THF solutions on a HPLC Lab Flow 2000 apparatus equipped with a Rheodyne 7725i injector, a Phenomenex Mixed bed column

5 μ MXL and a Linear Instruments UVIS-200 detector operating at 254 nm. The calibration curve was recorded using monodisperse polystyrene standards. A DSC TA Instruments Q2000 was used for the thermal analysis by varying the temperature from -50°C to 230°C at a rate of 5°C min⁻¹ in a nitrogen atmosphere. A TGA TA Instruments Q600, operating in air flux, was used to determine the decomposition temperatures of the samples by heating from 30°C to 900°C at a scan rate of 10°C min⁻¹. Cyclic voltammograms were recorded using an Autolab PGSTAT204 (Metrohm) potentiostat/galvanostat at a potential scan rate of 100 mV/s on polymer films deposited on Pt electrodes from chlorobenzene solutions. The working electrode (polymer coated Pt disk), the counter electrode (Pt wire) and the reference electrode (aqueous saturated calomel electrode) were immersed in an acetonitrile solution with tetrabutylammonium hexafluorophosphate (TBAPF₆) 0.1 M as supporting electrolyte using a single compartment three-electrode cell. AFM measurements were made on a Burleigh Vista 100 atomic force microscope in a semicontact tapping mode using high resolution silicon nitride tips. SEM characterizations were carried out on a Zeiss Evo 50EP Electronic Microscope. X-ray diffraction data of polymer films were recorded at room temperature by using a CuK α (λ = 1.5406 Å) radiation source (Philips PW 1050) and a Bragg-Brentano diffractometer (Philips PW 1710) equipped with a graphite monochromator in the diffracted beam. The 2 θ range between 2.0 and 90.0° was scanned by 881 steps of 0.1° with a counting time of 15 s for each step.

BHJ solar cells were prepared according to the following procedure: the ITO glass substrate (1 cm \times 1 cm, surface resistance 21 Ω /sq) was etched on one side by using a 10% wt aqueous solution of HCl and heated at 60°C for 15 min in order to obtain an area of 0.75 \times 1 cm covered by indium tin oxide. The glass was then cleaned in an ultrasonic bath (Elmasonic S30H) using acetone and then treated at 60°C for 20 min with a solution of aqueous NH₃ (0.8 M) and H₂O₂ (0.5 M), rinsed with distilled water, 2-propanol and dried with a nitrogen flow. The final resistance of the ITO glass was 12 Ω /sq. Poly(3,4-ethylenedioxythiophene):polystyrene sulfonic acid (PEDOT:PSS, 2.8 wt%

dispersion in water, viscosity 20 cps) was diluted 1:1 v/v with 2-propanol, sonicated, filtered on a Gooch G2 and the resulting solution (viscosity 12 cps) deposited over the previously treated ITO glass by the doctor blading technique using a Sheen Instrument Model S265674, leaving only a small (0.25×1 cm) area uncovered at the opposite side of the previously etched area. The PEDOT:PSS film was heated in a Büchi GKR-50 glass oven at 130°C for 2 h under vacuum (10^{-3} mmHg). A solution made by mixing 5 mg of PT6Br/F (or rrPT6Br/F) in 1 ml of chlorobenzene was sonicated for 15 min, filtered on a PTFE septum (0.25 μ m pore size) and deposited by doctor blading on the slide in order to cover the PEDOT:PSS layer. The sample was then annealed in the glass oven under vacuum (10^{-3} mmHg) at 120°C for 30 min. Finally, a 50 nm thick Al electrode was deposited over the polymeric layer through a shadow mask using an Edwards 6306A coating system operating at 10^{-6} mmHg. The active area of the cell was 0.25×0.25 cm². The current-voltage characteristics were measured in air using a Keithley 2401 source meter under the illumination of an Abet Technologies LS150 Xenon Arc Lamp Source AM 1.5 Solar Simulator (100 mW/cm²) calibrated with an ILT 1400-BL photometer. The structure of the final devices were: ITO (80 nm)/PEDOT:PSS (100 nm)/active layer (150 nm)/Al (50 nm). The spectral response of the solar cells was measured using a 7-SC Spec III Modularized Solar Cell Spectral Test System (SevenStar Optics, Beijing, PRC). Layer thicknesses were measured using a Film Thickness Probe FTPAdvances FTPadv-2 (Sentech GmbH, Germany) equipped with the FTPExpert software.

2.3. Monomer synthesis

2.3.1. 3-(6-bromohexyl)thiophene (T6Br)

73.6 ml (0.184 mol) of a 2.5 M solution of *n*-butyl-lithium in hexanes was added dropwise to a solution of 3-bromothiophene (30.0 g, 0.184 mol) in 250 ml of *n*-hexane previously cooled down to -80°C. After stirring for 10 min under argon atmosphere, 25 ml of anhydrous THF was added and

the mixture was stirred for 90 min and then warmed up to -10°C . 38 ml (0.247 mol) of 1,6-dibromohexane in 10 ml of anhydrous THF were then dropped and the mixture stirred for further 2 h at room temperature under inert atmosphere. The mixture was quenched with 200 ml of distilled water and extracted with 4×150 ml of diethyl ether. The organic phase was then washed to neutrality, dried over MgSO_4 and evaporated under reduced pressure to give 55.85 g of crude product which was purified by vacuum distillation to give 30.95 g of T6Br (68% yield), b.p. 96°C , 0.5 mmHg.

^1H -NMR (CDCl_3 , ppm): δ 7.24 (1H, m, $H5\text{Th}$); 6.93 (2H, m, $H2\text{Th}+H4\text{Th}$); 3.41 (2H, t, CH_2Br); 2.64 (2H, t, ThCH_2); 1.86 (2H, m, CH_2), 1.64 (2H, m, CH_2), 1.47 (2H, m, CH_2), 1.37 (2H, m, CH_2).

^{13}C -NMR (CDCl_3 , ppm): δ 143.57 (ThC3), 128.84 (ThC5), 125.32 (ThC2), 120.67 (ThC4), 34.41 (CH_2Br), 33.28 ($\text{CH}_2\text{CH}_2\text{Br}$), 30.87 (CH_2Th), 30.62 (CH_2), 29.03 (CH_2), 28.66 (CH_2).

FT-IR (KBr, cm^{-1}): 3104, 3049, 2924, 2856, 1537, 1465, 1435, 1246, 1215, 1080, 831, 768, 685, 634, 561.

2.3.2. 2,5-dibromo-3-(6-bromohexyl)thiophene (2,5BT6Br)

0.715 g (4.02 mmol) of N-bromosuccinimide (NBS) in 4.0 ml of N,N-dimethylformamide (DMF) were added dropwise – under stirring and in an inert atmosphere – to a solution of 1.00 g (4.02 mmol) of T6Br in 4.0 ml of DMF. The mixture was reacted for 6 h at room temperature in the dark and under a gentle argon flux. 1.07 g (6.02 mmol) of NBS in 6.0 ml of DMF were added dropwise and the mixture was reacted for another 24 h. The reaction mixture was then poured into 130 ml of an aqueous solution of NaCl and the organic phase was extracted with 5×100 ml of petroleum ether. The collected organic phases were washed with water to neutrality, dried and concentrated at reduced pressure giving 1.60 g (3.96 mmol) of 2,5BT6Br (98% yield).

$^1\text{H-NMR}$ (CDCl_3 , ppm): δ 6.77 (1H, s, $H^4\text{Th}$); 3.41 (2H, t, CH_2Br); 2.52 (2H, t, ThCH_2); 1.86 (2H, m, CH_2), 1.57 (2H, m, CH_2), 1.47 (2H, m, CH_2), 1.35 (2H, m, CH_2).

$^{13}\text{C-NMR}$ (CDCl_3 , ppm): δ 144.81 (ThC3), 133.29 (ThC5), 114.38 (ThC2), 111.21 (ThC4), 34.71 (CH_2Br), 33.36 ($\text{CH}_2\text{CH}_2\text{Br}$), 30.22 (CH_2Th), 29.18 (CH_2), 28.66 (CH_2), 28.13 (CH_2).

FT-IR (KBr, cm^{-1}): 3050, 2932, 2855, 1541, 1461, 1436, 1418, 1254, 1233, 1186, 1001, 826, 727, 645.

2.4. Polymer synthesis

2.4.1. Poly[3-(6-bromohexyl)thiophene] (PT6Br) by oxidative polymerization

2.68 g (16.5 mmol) of iron trichloride in 17 ml of anhydrous nitromethane was dropped in 20 min, under argon and at room temperature, into a solution of 1.00 g (4.02 mmol) of T6Br in 48 ml of anhydrous CHCl_3 . After the addition was completed, the reaction mixture was stirred for 2 h at room temperature and then added to 50 ml of THF. The mixture was then poured into 250 ml of a 5% methanolic solution of HCl and the resulting precipitate filtered on a PTFE membrane (0.45 μm pore size) and washed several times with further MeOH. The recovered polymer was then redissolved in 150 ml of CHCl_3 and the obtained solution washed with 2% aqueous HCl and with distilled water to neutrality. The organic phase was dried with MgSO_4 and concentrated at reduced pressure. The final polymer was fractionated using a 1:10 (v/v) $\text{CHCl}_3/\text{MeOH}$ mixture giving 0.392 g (40% yield) of dark-red PT6Br.

$^1\text{H-NMR}$ (CDCl_3 , ppm): δ 6.98 (1H, m, $H^4\text{Th}$); 3.43 (2H, m, CH_2Br); 2.83, 2.57 (2H, 2m, ThCH_2); 1.94-1.32 (8H, bm, CH_2).

^{13}C -NMR (CDCl_3 , ppm): δ 143.71, 143.01, 141.03, 140.28 (ThC3), 136.94, 135.88, 134.61, 134.77 (ThC5), 131.32, 130.85, 130.23, 129.85 (ThC2), 129.04, 128.65, 128.32, 127.63 (ThC4), 34.55 (CH_2Br), 33.81 ($\text{CH}_2\text{CH}_2\text{Br}$), 30.94 (CH_2Th), 29.96 (CH_2), 29.15 (CH_2), 28.53 (CH_2).

FT-IR (Ge, cm^{-1}): 3055, 2929, 2854, 1509, 1457, 1259, 1090, 827, 727, 645, 562.

Elemental analysis: Calcd. for $(\text{C}_{10}\text{H}_{13}\text{BrS})_n$: C 48.99; H 5.34; Br 32.59; S 13.08; Found: C 49.18; H 5.29; Br 32.65; S 12.88.

2.4.2. Poly[3-(6-bromohexyl)thiophene] (rrPT6Br) by GRIM (Grignard Metathesis) polymerization

1.40 ml of a 3.0M CH_3MgCl solution (4.20 mmol) in n-buthyl ether was added to 1.60 g (3.96 mmol) of 2,5BT6Br in 32 ml of anhydrous THF. The mixture was refluxed for 2 h under stirring and in inert atmosphere and then 10.7 mg (0.0198 mmol) of [1,3-bis(diphenylphosphino)propane] Nickel (II) chloride (NiDPPPCl_2) was added and the reaction refluxed for 75 min. After cooling down to room temperature, the mixture was poured in 400 ml of MeOH and the resulting suspension was centrifuged at 3000 rpm for 20 min. The recovered polymer was dissolved in 20 ml of CHCl_3 , filtered on a PTFE membrane (0.20 μm pore size) and fractionated using a 1:5 (v/v) $\text{CHCl}_3/\text{MeOH}$ mixture. After solvent evaporation at reduced pressure, 0.452 g (1.85 mmol) of reddish rrPT6Br were obtained (47% yield).

^1H -NMR (CDCl_3 , ppm): δ 6.98 (1H, s, $H^4\text{Th}$); 3.43 (2H, t, CH_2Br); 2.84 (2H, m, ThCH_2); 1.94-1.38 (8H, bm, CH_2).

^{13}C -NMR (CDCl_3 , ppm): δ 140.31 (ThC3), 134.91 (ThC5), 131.23 (ThC2), 129.01 (ThC4), 34.59 (CH_2Br), 33.97 ($\text{CH}_2\text{CH}_2\text{Br}$), 30.61 (CH_2Th), 29.83 (CH_2), 29.17 (CH_2), 28.55 (CH_2).

FT-IR (Ge, cm^{-1}): 3055, 2929, 2854, 1505, 1432, 1258, 1071, 826, 724, 642, 561.

Elemental analysis: Calcd. for $(\text{C}_{10}\text{H}_{13}\text{BrS})_n$: C 48.99; H 5.34; Br 32.59; S 13.08; Found: C 49.15; H 5.31; Br 32.42; S 13.12.

2.4.3. *Poly[3-(6-bromohexyl)thiophene-co-3-(6-fullerenylhexyl)thiophene]* (PT6Br/F) by *post-functionalization of PT6Br*

0.200 g (0.816 mmol) of PT6Br in 5 ml of anhydrous THF was added dropwise to 14.87 mg (0.612 mmol) of Mg turnings under stirring and in an inert atmosphere. The mixture was refluxed for 20 h, cooled down to room temperature, and then transferred via cannula to a solution of 0.441 g (0.612 mmol) of C₆₀-fullerene in 300 ml of anhydrous toluene and 1.3 ml of anhydrous N,N-dimethylformamide (DMF). The reaction mixture was stirred for 90 min under inert atmosphere and then 2.5 ml of a 1.87 M aqueous solution of NH₄Cl and 100 ml of brine was added. The organic phase was washed several times with distilled water, dried with MgSO₄ and concentrated. The copolymer was dissolved in 100 ml of CHCl₃ and the obtained solution dropped into 350 ml of *n*-heptane. After filtration on a PTFE membrane (0.45 μm pore size), 0.407 g (0.609 mmol) of fractionated PT6Br/F was obtained (75% yield).

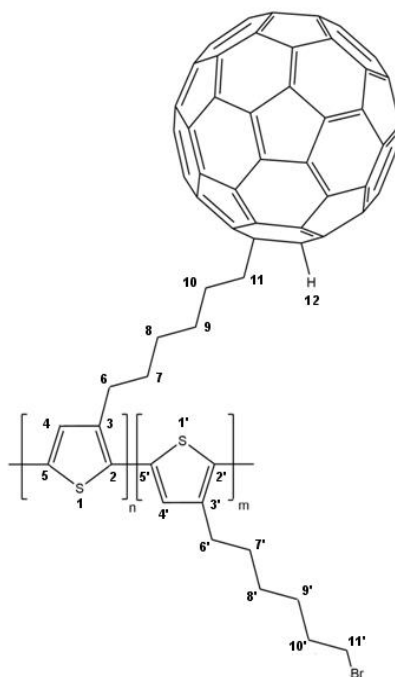


Figure 1. Atoms numbering for copolymers

$^1\text{H-NMR}$ (pyridine- d_5 , ppm): δ 7.47 (m, H4+H4'); 7.38 (s, H12); 3.58 (m, H11); 3.45 (m, H11'); 3.01, 2.81 (m, H6+H6'); 1.91-1.14 (bm, H7+H8+H9+H10+H7'+H8'+H9'+H10').

$^{13}\text{C-NMR}$ (ODCB- d_4 , ppm): δ 160.03 (C_{60}), 156.28 (C_{60}), 151.67 (C_{60}), 149.29 (C_{60}), 148.36 (C_{60}), 147.94 (C_{60}), 147.81 (C_{60}), 147.38 (C_{60}), 146.99 (C_{60}), 146.12 (C_{60}), 146.01 (C_{60}), 145.89 (C_{60}), 145.55 (C_{60}), 145.38 (C_{60}), 145.24 (C_{60}), 145.01 (C_{60}), 144.77 (C_{60}), 144.12 (C_{60}), 143.79 (C_{60}), 143.47 (C_{60}), 142.66 (C_{60}), 142.14 (C_{60}), 142.03 (C_{60}), 141.91 (C_{60}), 141.73 (C_{60}), 141.22 (C_{60}), 143.48, 142.96, 141.12, 140.57 (C3+C3'), 140.29 (C_{60}), 140.04 (C_{60}), 137.75 (C_{60}), 136.04 (C_{60}), 136.65, 136.02, 135.55, 134.95 (C5+C5'), 129.82, 129.78, 129.52, 129.26 (C2+C2'), 129.11, 128.88, 128.36, 128.03 (C4+C4'), 61.76 (C11), 42.95 (C10), 34.73 (C11'), 34.02 (C10'), 30.68 (C6+C6'), 29.95 (C9+C9'), 29.32 (C7+C7'), 28.73 (C8+C8').

FT-IR (KBr, cm^{-1}): 3053, 2929, 2852, 1506, 1455, 1429, 1260, 1182, 1034, 834, 747, 649, 576, 560, 522.

Elemental analysis: Calcd. for $[(\text{C}_{70}\text{H}_{14}\text{S})_{0.66} (\text{C}_{10}\text{H}_{13}\text{BrS})_{0.34}]$: C 89.08; H 2.06; Br 4.06; S 4.80; Found: C 89.33; H 1.98; Br 3.83; S 4.86.

2.4.4. Poly[3-(6-bromohexyl)thiophene-co-3-(6-fullerenylhexyl)thiophene] (rrPT6Br/F) by post-functionalization of rrPT6Br

The adopted procedure was the same as for PT6Br/F, using 0.200 g (0.816 mmol) of rrPT6Br in 10 ml of anhydrous THF and 4.90 mg (0.202 mmol) of Mg turnings for the Grignard formation, and 0.147 g (0.204 mmol) of C_{60} -fullerene in 100 ml of anhydrous toluene and 0.5 ml of anhydrous N,N-dimethylformamide (DMF) for the coupling step. 0.250 g (0.776 mmol) of fractionated rrPT6Br/F was obtained (95% yield).

¹H-NMR (pyridine-d₅, ppm): δ 7.47 (s, H4+H4'); 7.38 (s, H12); 3.58 (m, H11); 3.47 (m, H11'); 3.02, 2.78 (m, H6+H6'); 1.89-1.12 (bm, H7+H8+H9+H10+H7'+H8'+H9'+H10').

¹³C-NMR (ODCB-d₄, ppm): δ 159.89 (C₆₀), 156.26 (C₆₀), 151.59 (C₆₀), 149.24 (C₆₀), 148.32 (C₆₀), 147.89 (C₆₀), 147.80 (C₆₀), 147.37 (C₆₀), 146.95 (C₆₀), 146.08 (C₆₀), 145.99 (C₆₀), 145.77 (C₆₀), 145.42 (C₆₀), 145.26 (C₆₀), 145.18 (C₆₀), 145.00 (C₆₀), 144.74 (C₆₀), 144.11 (C₆₀), 143.76 (C₆₀), 143.43 (C₆₀), 142.64 (C₆₀), 142.11 (C₆₀), 142.01 (C₆₀), 141.86 (C₆₀), 141.69 (C₆₀), 141.18 (C₆₀), 140.55 (C3+C3'), 140.21 (C₆₀), 140.00 (C₆₀), 137.77 (C₆₀), 136.02 (C₆₀), 134.93 (C5+C5'), 129.81 (C2+C2'), 128.88 (C4+C4'), 61.75 (C11), 42.93 (C10), 34.72 (C11'), 34.00 (C10'), 30.67 (C6+C6'), 29.95 (C9+C9'), 29.30 (C7+C7'), 28.71 (C8+C8').

FT-IR (KBr, cm⁻¹): 3056, 2930, 2852, 1513, 1456, 1428, 1259, 1182, 1031, 836, 749, 646, 576, 562, 525.

Elemental analysis: Calcd. for [(C₇₀H₁₄S)_{0.12} (C₁₀H₁₃BrS)_{0.88}]: C 64.12; H 4.10; Br 21.82; S 9.96; Found: C 64.29; H 4.02; Br 21.77; S 9.92.

2.5. Preparation of gold nanoparticle layer

Gold nanoparticle (AuNPs) layer was prepared according to Ref. [19,20]. 3.30 mg (8.4 μmol) of Gold(III) chloride hydrate (HAuCl₄·3H₂O, Aldrich Cod. 254169) were dissolved in 10 ml of distilled water and added with 2 ml of H₂O₂ (30% w/v). The volume of the solution was halved by heating and the obtained solution was sonicated, filtered on a PTFE septum (0.20 μm pore size) and 400 μl of the resulting solution was deposited using a BLE Spin Coater operating at 2000 rpm on the ITO glass slide previously spin-cast using the PEDOT:PSS solution and allowed to dry into a temperature-controlled oven at 75°C. The final thickness of the AuNPs layer was around 30 nm.

3. Results and discussion

3.1. Polymers synthetic strategy

The adopted procedure for the preparation of PT6Br/F (and rrPT6Br/F) from the corresponding homopolymers PT6Br (and rrPT6Br) is shown in Scheme 1. PT6Br was synthesized by reacting 3-(6-bromohexyl)thiophene with iron trichloride in $\text{CH}_3\text{NO}_2/\text{CHCl}_3$ mixture, with a procedure involving precipitation of the oxidizing agent in a highly active microcrystalline form, in order to minimize the insoluble fraction content by the control of the polymer molecular weight [21]. rrPT6Br was instead polymerized by means of a regiospecific procedure, namely the Grignard Metathesis (GRIM) polymerization, which involved the cross-coupling of the organomagnesium intermediate prepared by reacting 2,5-dibromo-3-(6-bromohexyl)thiophene (2,5BT6Br) with a pre-formed Grignard reactive (CH_3MgCl) in the presence of NiDPPPCl_2 catalyst. PT6Br and rrPT6Br were well soluble in common organic solvents and this was particularly true for the regioirregular sample (up to 50 mg/ml and 20 mg/ml in THF for PT6Br and rrPT6Br, respectively). The brominated homopolymer characteristics are reported in Table 1.

Table 1. Homopolymers and copolymers characteristics

Sample	Yield ^a (%)	HT dyads ^b (%)	M_n^c (KDa)	M_w/M_n^c	Fullerene content ^d (mol%)
PT6Br	40	70	26	1.37	0
rrPT6Br	47	96	24	1.33	0
PT6Br/F	75	70	71 ^e	1.37 ^e	66
rrPT6Br/F	95	97	31 ^e	1.33 ^e	12

^a In fractionated polymer

^b Regioregularity from ^1H -NMR expressed as head-to-tail dyads percentage

^c Determined by GPC relative to polystyrene standards

^d Determined by ¹H-NMR

^e Calculated from the molecular mass of the corresponding homopolymers

The homopolymers were then dissolved in anhydrous THF and added with Mg turnings to obtain the corresponding ω -bromomagnesium derivatives which were directly reacted with a solution of fullerene in toluene. The obtained copolymers were well soluble in chlorobenzene (CB), 1,2-dichlorobenzene (ODCB) and pyridine up to 10 mg/ml but only partially soluble in CHCl₃ and THF (around 0.5 mg/ml). The solubility of rrPT6Br/F in common organic solvents is almost the same of its regioirregular counterpart despite the lower molecular weight and fullerene content. This can be ascribed to the higher degree of regioregularity (and then of molecular packing) of rrPT6Br/F, strongly hindering solvation of the macromolecular structure.

3.2. FT-IR characterization

The FT-IR bands of homopolymers (PT6Br and rrPT6Br) and copolymers (PT6Br/F and rrPT6Br/F) as well as their assignments are reported in Table 1 SI.

The PT6Br spectrum shows the absence of the bands at 3104 cm⁻¹ (ν C-H in α to thiophene ring) and 768 cm⁻¹ (γ C-H 3-substituted thiophene), clearly evident in monomer T6Br, while the rrPT6Br spectrum reveals the absence of the band at 1001 cm⁻¹ (ν C-Br aromatic), present in 2,5BT6Br, thus confirming the formation of polymers at high molecular weight. Moreover, the presence of the absorptions at 1429, 1182, 576 and 522 cm⁻¹ in PT6Br/F and at 1428, 1182, 576 and 525 cm⁻¹ in rrPT6Br/F spectra, ascribable to C₆₀-fullerene, confirms the expected substitution in the side chains.

It can also be observed (Figure 2) that the intensity of fullerene absorptions is roughly proportional to its content in the copolymer.

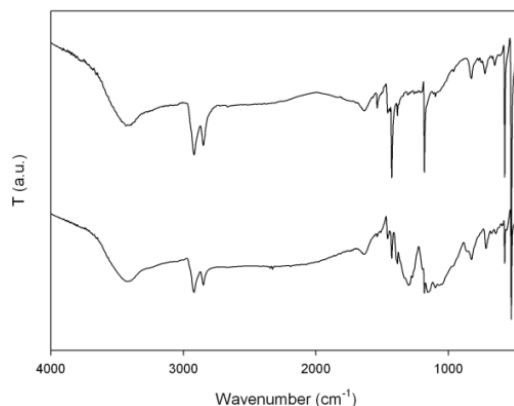


Figure 2. FT-IR spectra of PT6Br/F (top) and rrPT6Br/F (bottom)

3.3. NMR characterization

The ^1H -NMR spectra of the copolymers in d_5 -pyridine are reported in Figure 3.

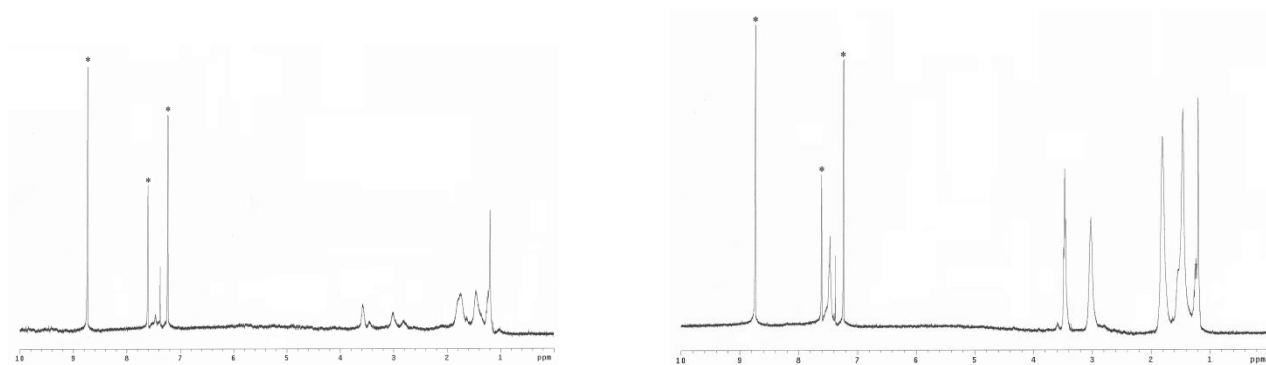


Figure 3. ^1H -NMR spectra of PT6Br/F (left) and rrPT6Br/F (right). Asterisk: solvent resonances.

The spectra show two signals in the aromatic region, at 7.47 and 7.38 ppm, which are ascribable to the H-4 thiophenic proton and to the proton directly attached to fullerene group, respectively. The signals at 3.58 and 3.45 (3.47 for rrPT6Br/F) ppm, ascribable to the methylenic protons α - to C_{60} and Br group, were used to calculate the fullerene content (66% and 12% molar ratio in PT6Br/F

and rrPT6Br/F, respectively). The resonance of methylenic protons α to thiophene ring is split into two signals (at 3.01 and 2.81 ppm for COP and at 3.02 and 2.78 ppm for rrPT6Br/F) ascribable to the dyads originating from different monomer couplings: the peak at lower fields may be assigned to head-to-tail (HT) junctions, while the other one to head-to-head and tail-to-tail (HH, TT) junctions. The regioregularity of polymers is thus given by the ratio of their integrated intensities: 70% HT for PT6Br/F and 97% HT for rrPT6Br/F, in agreement with the values usually reported for oxidative polymerization and GRIM polymerization of alkylthiophene monomers, respectively [22].

^{13}C -NMR spectra of PT6Br/F and rrPT6Br/F in d_4 -o-dichlorobenzene (ODCB) and are reported in Figure 4.

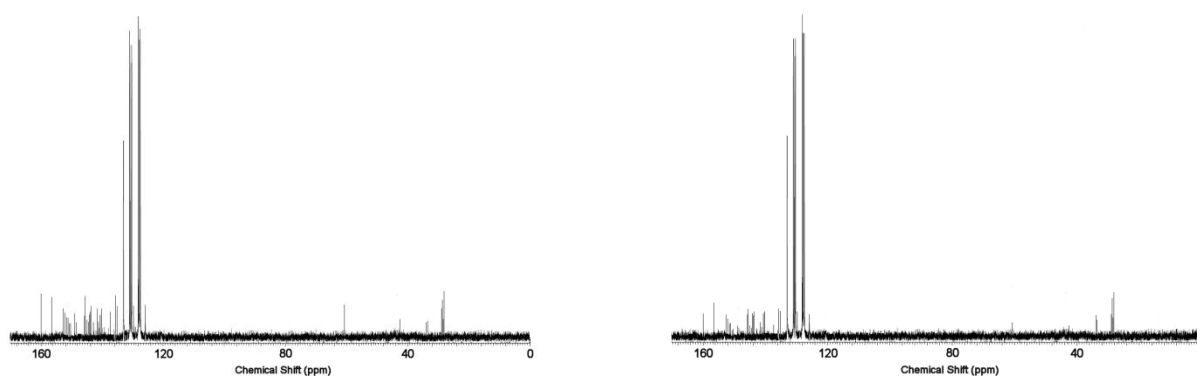


Figure 4. ^{13}C -NMR spectra of PT6Br/F (left) and rrPT6Br/F (right).

The signals at 127.19, 130.04, 132.39 ppm are originated by ODCB. As detailed in the Experimental section, the spectra show the signals ascribable to the 3-(6-bromohexyl)thiophene and 3-(6-fullerenylhexyl)thiophene units and the intensity of the signals of the latter unit is lower in rrPT6Br/F, according to its lower fullerene content. Moreover, the prevalence of only four evident signals related to thiophenic carbons in rrPT6Br/F ^{13}C -NMR spectrum further confirms the prevalence of one kind of configurational sequence (HT-HT) in this copolymer, as already observed by ^1H -NMR analysis.

3.4. UV-Vis analysis

Figure 5 shows the UV-Vis spectra of PT6Br/F and rrPT6Br/F in film on quartz slide (from chlorobenzene solution).

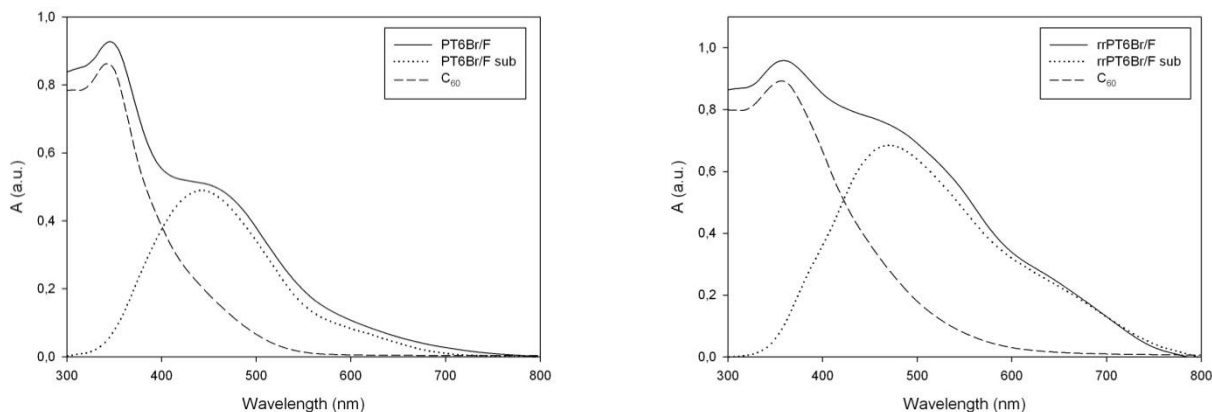


Figure 5. UV-Vis spectrum of PT6Br/F (left) and rrPT6Br/F (right) in film.

The evident absorbance around 350 nm is ascribable to fullerene, which is a very efficient chromophore particularly at lower wavelengths [23]. With the aim of better evaluate the absorption of the polythiophenic component, an UV-Vis spectrum of fullerene (C_{60}) has been recorded in chlorobenzene (CB) solution and subtracted from the copolymers spectra in order to detect the absorption of polythiophenic moieties at higher wavelengths. The analysis of the subtracted spectra (PT6Br/F sub and rrPT6Br/F sub) gives the absorption maximum for the polythiophenic component: 448 nm for PT6Br/F and 468 nm for rrPT6Br/F, corresponding to an average conjugation length of 6 and 8 thiophenic rings, respectively [24]. Moreover, the spectrum of rrPT6Br/F shows a shoulder at 632 nm (visible at around 620 nm in PT6Br/F spectrum), ascribable to the 0-0 pure electronic transition, which is only evident in conformationally ordered polythiophenic chains, giving interchain π - π stacking in the solid state [25]. Clark et al. [26] determined the exciton bandwidth W from the ratio of the 0-0 (pure electronic transition) and 0-1 (first vibronic quantum) peak absorbance in rrP3HT films. W is an important parameter, since it is related to the conjugation length and intrachain order in polyalkylthiophenes [27,28]. Unfortunately,

the 0-1 vibronic transition is not clearly evident in PT6Br/F and rrPT6Br/F film spectra, thus the copolymer morphology has been analyzed by the method discussed by Yamamoto et al. [29]. According to their theory, the UV-Vis film spectrum of functionalized polyalkylthiophenes can be separated in two essential contributions: the absorption at around 450 nm (A_a), ascribable to the amorphous domains, and the vibrational absorption shoulders at around 620-630 nm (A_c), due to the π - π stacking of polymer chains in crystalline domains. The degree of crystallinity, related to the degree of order of the polymer chains in the solid (film) state, can be roughly estimated using the following equation:

$$\chi_c = \frac{(\varepsilon_a/\varepsilon_c)A_c}{(\varepsilon_a/\varepsilon_c)A_c + A_a} \quad (1)$$

where $\varepsilon_a/\varepsilon_c$ (0.719) is the extinction coefficient ratio between the amorphous and crystalline poly(3-hexylthiophene) [29]. From the reported spectra, being A_c 0.08 and 0.26 and A_a 0.47 and 0.68 for the non regioregular and the regioregular sample, respectively, a degree of crystallinity of 11% and 22% can be estimated for PT6Br/F and rrPT6Br/F. As a result, the regioregular copolymer is more prone to assume ordered conformations leading to aggregates suited to give crystallization.

3.5. Electrochemical characterization

The copolymers have been electrochemically characterized by cyclic voltammetry (CV) using polymer-coated Pt disk as the support electrode, acetonitrile containing TBAPF₆ as supporting electrolyte, Pt wire as counter electrode and SCE as reference electrode. Copolymers films display an onset of the p-doping process at 0.83 V (PT6Br/F) and 1.22 V (rrPT6Br/F) with a faster increase

of the oxidation current for the latter, suggesting a better conductivity and, therefore, improved performance when employed as electron-donor polymer (Figure 6).

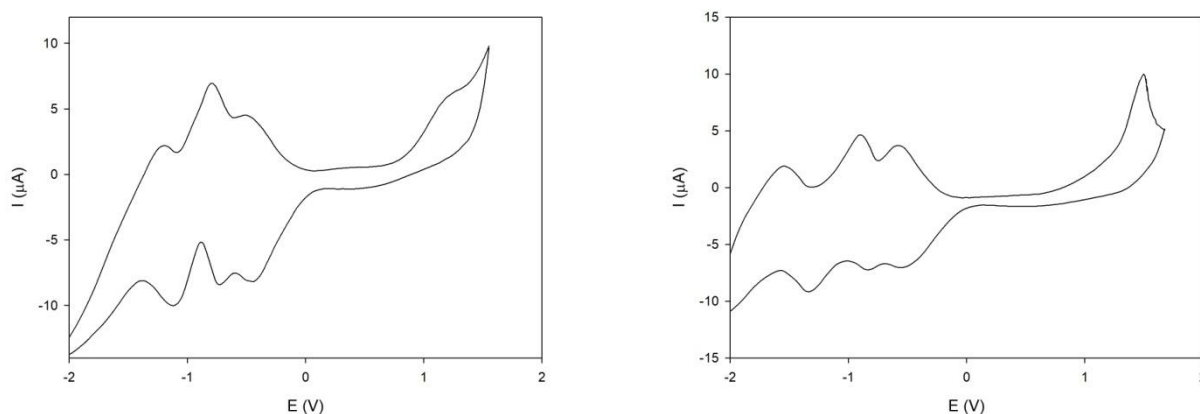


Figure 6. CV curves (third cycle) recorded in 0.1 M TBAPF₆/acetonitrile solution at 0.05 V/s for a Pt electrode coated with PT6Br/F (left) and rrPT6Br/F (right).

The HOMO level of the copolymers was measured by CV while the LUMO energy was calculated indirectly, since the negative potentials zone of the voltammograms was dominated by several waves ascribable to the multiple reduction processes of the fullerene group [30] making impossible to evaluate the reduction potential of the polythiophenic component of the films. However, the electrochemical behavior of the films indicates that both the fullerene pendant group and the conjugated polythiophene chain retain their individual electrochemical properties. Considering that the SCE reference electrode has a potential of 4.40 eV relative to vacuum [31], the energy of the HOMO levels was then estimated according to the relation:

$$I_p(\text{HOMO})(\text{eV}) = -e(E_{\text{ox}}^{\text{onset}} + 4.40)$$

The energy of the LUMO levels was calculated from the HOMO values and the values of the optical bandgaps (E_g^{opt}) obtained from the UV-Vis of films, by means of the following relation:

$$\text{LUMO} = \text{HOMO} + E_g^{\text{opt}} \text{ (eV)}$$

As reported in Table 2, rrPT6Br/F shows a HOMO level energy particularly low if compared with the standard reference P3HT (-4.8 eV [32]) and this is favorable for the obtainment of high open-circuit voltage, being the V_{oc} of a BHJ solar cell directly proportional to the absolute value of $I_p(\text{HOMO})$ [33]. Moreover, the regioregular copolymer bandgap results also very low, with positive potential implications on the conversion efficiency of the cell [34].

Table 2. Copolymer electrochemical characteristics

Sample	$E_{\text{ox}}^{\text{onset}}$ (V)	E_g^{opt} (eV)	HOMO (eV)	LUMO (eV)
PT6Br/F	0.83	2.04	-5.23	-3.19
rrPT6Br/F	1.22	1.83	-5.62	-3.79

3.6. Thermal properties

The thermal stability of copolymers was determined by TGA under oxidizing atmosphere (air) at a heating scan of 10°C/min (Figure 1 SI). PT6Br/F is thermally stable up to 271°C and rrPT6Br/F up to 236°C (Table 3). The observed weight loss can be ascribed to HBr and CH₂Br losses, and is more evident for the regioregular sample as a consequence of its higher bromine content, while the polythiophenic main chains are stable up to about 500°C. The DSC analysis was carried out under nitrogen atmosphere with a heating rate of 5°C/min (Figure 2 SI). The polymeric samples show glass transitions and melting points at temperatures increasing with the bromine content. Only rrPT6Br/F shows a clear first order crystallization transition, suggesting that the presence of a high amount of the sterically-hindering fullerene, together with a lower degree of configurational regularity, favors higher prevalence of amorphous structures in PT6Br/F.

Table 3. Glass-transition (T_g), melting (T_m), crystallization (T_c) and decomposition (T_d) temperatures of copolymers.

Sample	T_g (°C)	T_m (°C)	T_c (°C)	T_d (°C)
PT6Br/F	26	82	-	271
rrPT6Br/F	31	96	92	236

3.7. Morphological analysis

Figure 3 SI exhibits XRD patterns of PT6Br/F and rrPT6Br/F in film before and after the annealing procedure obtained under the same experimental conditions adopted for the preparation of solar cells (i.e. heating in the glass oven under vacuum at 120°C for 30 min).

The annealed samples show slightly sharper and more intense peaks than the pristine ones, proving the effectiveness of the annealing procedure in enhancing the structural order of the functionalized polythiophenic system. All the examined samples show small angle reflections in the $2\theta=3.75-4.67$ range, corresponding to the first order reflections (100) ascribable to the distance between polythiophenic chains lying on the same plane (Table 4). PT6Br/F and rrPT6Br/F films also show the second order reflections (200) which are determined by the multiple X-ray reflections by the film. Only for the regioregular sample the third order reflections (300) can be found, indicating the attainment of an improved structural order induced by the higher configurational regularity. The interlayer d_I spacings distances are notably lower in the annealed samples, confirming the positive effect of the annealing procedure on the structural order and on the packing degree of the copolymer films.

Table 4. Structural parameters of the synthesized copolymers in film

Sample	Low-angle	On plane PT chain
	diffractions	distances
	(2 θ , degree)	(Å)
PT6Br/F	3.75; 7.63	23.55
PT6Br/F ann.	3.84; 7.72	22.98
rrPT6Br/F	4.61; 9.31; 13.90	19.13
rrPT6Br/F ann.	4.67; 9.38; 14.12	18.92

The surface morphology of the copolymers was examined by AFM. The films had similar thickness (about 100 nm) and were obtained by filming with doctor blade the CB solutions of polymers on ITO glasses. The annealed samples were subjected to the same procedure described for XRD analysis. The AFM images (Figure 7) are similar, showing the formation of an homogeneous bi-continuous network between the brighter and the darker areas (determined by the polythiophene- and the fullerene-rich phases, respectively), as expected from the molecular architecture, providing the covalent linking of the EA group directly to the polyconjugated backbone. Moreover, the effect of the annealing procedure on the film morphology can be evaluated considering the root-mean-square (RMS) roughness of the different samples, which increases from 1.08 to 1.13 nm for PT6Br/F and from 0.89 to 1.05 nm for rrPT6Br/F. The films surface becomes rougher since controlled heating enhances the crystallinity of the polythiophenic component of the double-cable polymer [35,36], with positive effects on the hole-carrier transport [37].

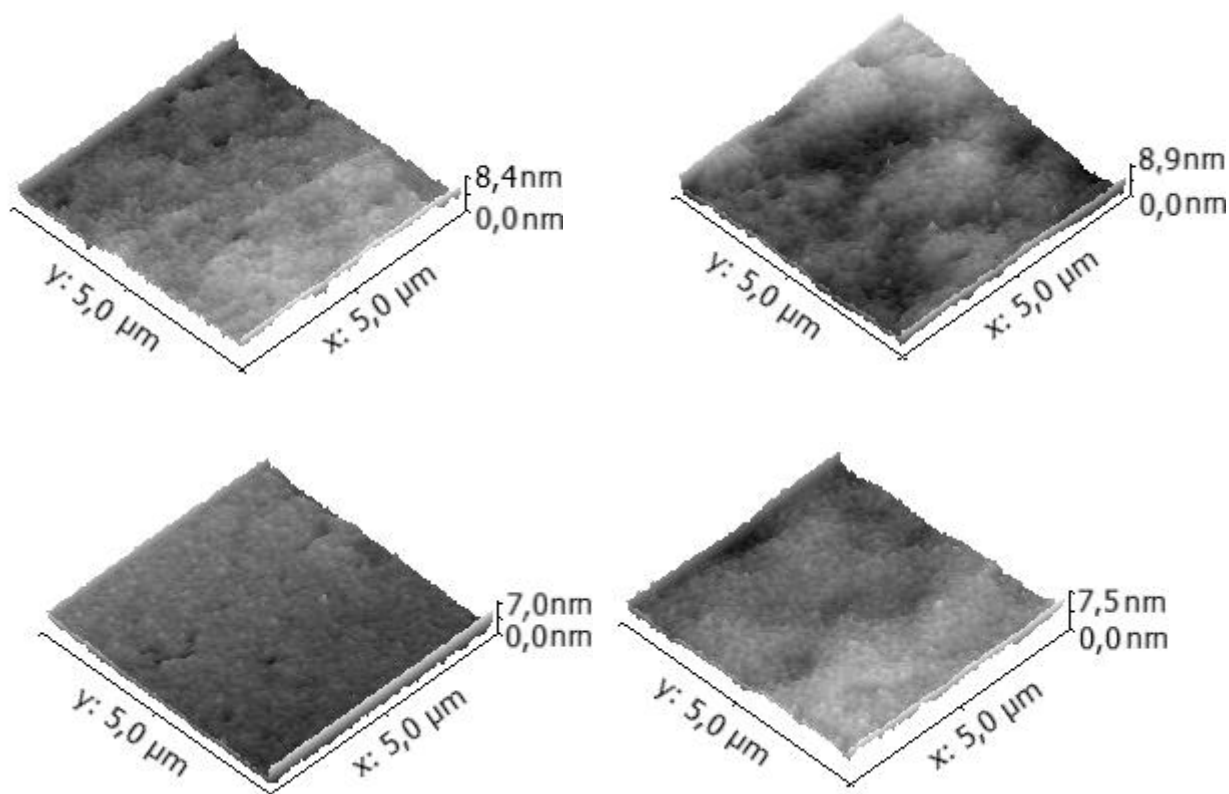


Figure 7. AFM images of PT6Br/F (top) and rrPT6Br/F (bottom) film surfaces; left: before annealing, right: after annealing.

We have also synthesized gold nanoparticles (AuNPs) to be used as an anode interlayer in the polymeric cells according to the preparation described in the Experimental section.

The SEM image indicates that the mean size of AuNPs is 13.5 ± 3.3 nm while the root-mean-squared (RMS) roughness, determined by AFM, is measured to be 5.5 ± 0.5 nm (Figure 4 SI). It is noteworthy that the sheet electric resistance of PEDOT:PSS layer was $200 \Omega/\text{sq}$, while that of AuNPs was only $10 \text{ m}\Omega/\text{sq}$.

3.8. Photovoltaic properties

A series of PSCs with the structure ITO (80 nm)/PEDOT:PSS (100 nm)/double-cable copolymer (150 nm)/Al (50 nm) has been fabricated under the conditions described in the Experimental

section, with the aim to investigate the performance of the synthesized copolymers as photoactive layers. Current density-voltage curves of the devices are shown in Figure 8 and the key photovoltaic parameters (short-circuit current density J_{SC} , open-circuit voltage V_{OC} , fill factor FF and power conversion efficiency PCE) are summarized in Table 5. The regioregular copolymer shows a PCE notably higher than its regioirregular counterpart (5.21 vs 3.55%) despite its lower fullerene content, owing to increased crystallinity and reduced bandgap. The structural regularity appears then a key-parameter to promote the formation of efficient bi-continuous interpenetrating networks able to enhance the charge transport to the electrodes and their subsequent collection, as demonstrated by the higher value of J_{SC} obtained with rrPT6Br/F sample. Moreover, the regioregular sample also shows a higher value of V_{OC} , according to its lower HOMO level energy. The obtained results are in good agreement with the findings reported by Malik et al. in a recent work [38], in which the importance of structural regioregularity in the donor polymer is evidenced. The authors observed that highly regioregular ED-polymers show an enhanced mobility of excitons and a compressed bandgap, which can improve the absorption efficiency of the solar spectrum.

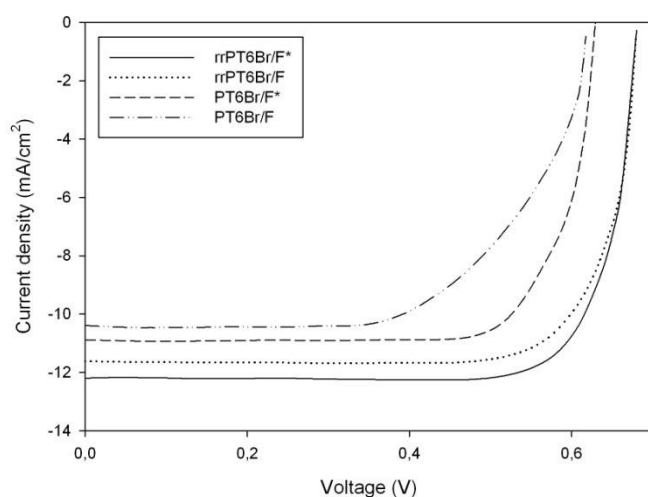


Figure 8. Current density-voltage for the best-performing cells under AM 1.5 one-sun illumination.

Table 5. Photovoltaic characteristics of the obtained devices

Sample	J_{sc} (mA cm ⁻²) ^a	V_{oc} (V) ^a	FF ^a	PCE (%) ^a
rrPT6Br/F	11.6±1.2	0.68±0.01	0.64±0.03	5.21±0.09
rrPT6Br/F*	12.2±1.3	0.68±0.01	0.67±0.04	5.68±0.12
PT6Br/F	10.4±1.1	0.62±0.01	0.55±0.06	3.55±0.13
PT6Br/F*	10.9±1.2	0.63±0.01	0.60±0.05	4.12±0.08

^a Average values collected from ten devices.

* Samples with AuNPs interlayer.

The wavelengths of photocurrent response for the cells based on copolymer films range from 300 to 710 nm; the curve of the device based on PT6Br/F sample has two feature peaks at 330 and 540 nm, whereas the device prepared with rrPT6Br/F shows two main peaks at 350 and 560 nm (Figure 9). The quantum efficiency (EQE) profiles substantially follow the trend observed in the absorption spectra of copolymers in film, suggesting that the harvested photons over the whole absorption spectrum can effectively contribute to the final photocurrent. Moreover, enhanced EQE is observed with the device made with the regioregular double-cable copolymer (EQE_{max} 68% vs 59%), indicating an improved charge collection efficiency for rrPT6Br/F, in agreement with the higher value of J_{sc} recorded for this sample when used as photoactive layer in BHJ solar cell. The parameters derived from EQE measurements [39] (J_{sc} , $J_{sc, max}$ with a theoretical 100% EQE and HOMO-LUMO bandgap) are in good agreement with the above reported values (12.1 mA cm⁻², 19.4 mA cm⁻², 1.85 eV for rrPT6Br/F and 10.8 mA cm⁻², 18.3 mA cm⁻², 1.96 eV for PT6Br/F, respectively).

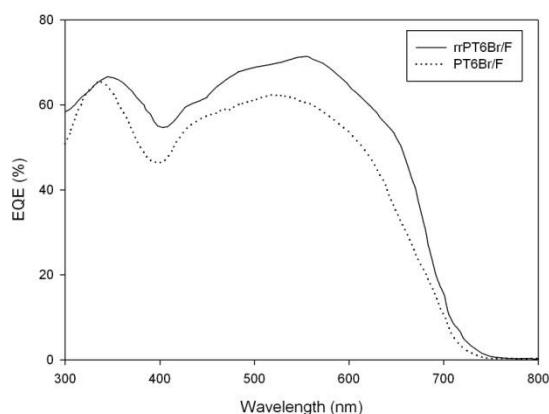


Figure 9. EQE spectra of copolymer devices.

In order to further enhance the current density of the prepared devices, a thin layer of AuNPs has been inserted between the PEDOT:PSS and the photoactive blend. It is in fact well known that the presence of a highly-conductive interlayer in BHJ polymeric solar cells can help to reduce the series resistance [40,41]. The solar cells with the NPs interlayer were thermally-treated and measured similarly to those previously described, giving the J/V curves reported in Fig. 8 and the photovoltaic performances reported in Table 5 (samples PT6Br/F* and rrPT6Br/F*). Their architecture was: ITO (80 nm)/PEDOT:PSS (100 nm)/AuNPs (30 nm)/double-cable copolymer (150 nm)/Al (50 nm).

The comparison of the values reported in Table 5 indicates that, after incorporating AuNPs interlayer, the PCE increased by about 11% as a result of the increased J_{sc} and FF values, thus proving the effectiveness of the metal nanoparticles layer in reducing the series resistances and increasing the charge mobility. The obtained results suggest that the insertion of a thin interlayer of metallic NPs can be a simple and effective method to enhance the efficiency of polymeric BHJ solar cells.

3.9. Photocrosslinking of photoactive layers

The importance of thermal annealing for the optimization of photoactive layer morphology was first reported by Padinger et al. [42] on P3HT/PCBM blends. Heating the active layer of the OPV cell to a temperature higher than T_g (or T_m , when detectable) allows the polymer chains to reorganize in a more crystalline structure and the fullerene molecules to diffuse into the blend and reorder in a more thermodynamically favorable way. Annealing generally results in higher photons to charges conversion at all wavelengths across the polymer blend absorption spectrum and in enhanced mobility of the charge carriers [43]. However, the bicontinuous network with nanometer-scale phase segregation created in the blend after the annealing procedure is not thermally-stable over time, since the polymer-fullerene nanoclusters are intrinsically thermodynamically unstable, being created by kinetically trapping the electron donor/acceptor nanostructures. The consequence of this is that during the light exposition of the final devices (or after long storing times), the two components spontaneously tend to segregate, giving the original macrophase separation. In order to enhance the phase stability of the BHJ solar cells, some authors proposed the adoption of thermally cross-linkable moieties on the polymer chains [44,45] but they observed a decrease of PCE ascribable to the attainment of a more disordered blend morphology during the thermal crosslinking procedure. A valuable alternative to thermal crosslinking can be the photocrosslinking since it can be performed at room temperature. This procedure has been applied to our copolymers, being functionalized with bromine groups which can be crosslinked via a radical mechanism initiated by the photochemical cleavage of C-Br bonds under UV-light [46,47]. The photocrosslinking was carried out on the just annealed BHJ cells, before Al cathode deposition, using a Philips UV-C PL 11W lamp (3.2W @ 250 nm, λ_{max} at 253.7 nm, distance of irradiation 5 cm) with an exposure time of 30 min. The right irradiation time was determined by exposing the films to UV-light for different times; the exposed films were then immersed in CB for 15 min, rinsed with methanol and dried. The films weights before and after CB treatment were then compared. After 15 min of UV exposure

the copolymers films were totally insoluble in the chlorinated solvent, proving the effectiveness of the crosslinking procedure.

The thermal stability was studied using the most performing cells (samples PT6Br/F* and rrPT6Br/F*) with a conventional P3HT:PCBM blend device as a control sample. The architecture of the reference cell was: ITO/PEDOT:PSS/AuNPs/P3HT ($M_n = 36$ KDa, PDI = 1.25, 96% HT):PCBM (1:1 w/w)/Al. The cells were submitted to constant heating at 150°C under vacuum for different times (up to 80 h) in order to simulate an accelerated aging (Figure 10).

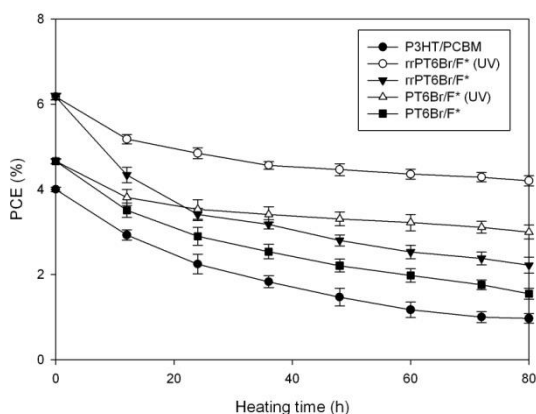


Figure 10. Efficiencies of OPV cells heated at 150°C vs. time. The devices were prepared under the same experimental conditions except for UV exposure (30 min) and five devices of each kind were tested.

The PCE of the unexposed samples decreases to a 36% (rrPT6Br/F*) and 34% (PT6Br/F*) of the initial value after 80 h at 150°C while the reference cell exhibits a faster decrease, reaching the 25% of the initial efficiency. The measurements confirm the intrinsic higher stability of photoactive layers made of single material double-cable copolymers when compared to the conventional polymer/PCBM blend architecture. The covalent linkage of the EA moiety to the polymer (ED) structure gives a beneficial impact on duration and thermal properties of the final device by

reducing the mobility of the components. The effectiveness of the photocrosslinking procedure is evidenced by the results obtained with the UV-exposed samples, which showed very stable device performances even after 80 h of annealing at 150°C (68% and 65% of the initial device efficiency for the regioregular and the non-regioregular copolymer, respectively). The obtained results clearly evidence that the photocrosslinking procedure is particularly promising for the achievement of thermally stable high performance devices.

4. Conclusions

Two photocrosslinkable thiophene copolymers with different configurational order have been prepared with the aim to prepare high performance single component organic photovoltaic solar cells. The new double-cable donor-acceptor polythiophene derivatives have been successfully synthesized using a facile and effective postpolymerization approach on poly[3-(6-bromohexylthiophene)] (PT6Br) by means of a Grignard coupling reaction with C₆₀-fullerene. The successful anchorage of C₆₀ to the PT6Br backbone was confirmed by FT-IR, NMR and elemental analysis which also allowed to determine the substitution degree. The two precursor polymers showed similar molecular weights but different degrees of regioregularity and were functionalized with different amounts of fullerene, according to their different solubility. The regioregular sample showed the most performing properties despite its lower content of EA group, confirming the decisive effect of the structural regularity on the electronic characteristics of the photoactive blend. A notable increase in power conversion efficiency was obtained by interposing a thin layer of Au nanoparticles between the buffer and the photoactive layer, allowing to reach a PCE of 5.68% with the regioregular sample. Finally, the stability of the prepared OPV cells can be improved through the photocrosslinking of the brominated side chains. The simplicity of the proposed synthetic approach, together with the especially tailored functional groups inserted in the terminal position of the side-chains, provide a new versatile architecture for the construction of efficient donor-acceptor

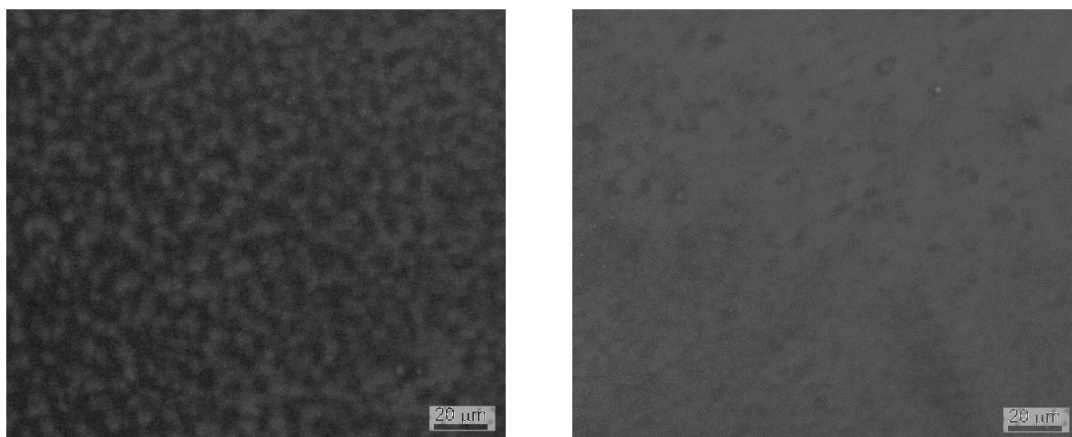
intramolecular polymeric hybrids which can be further exploited for the construction of single material photoactive layers.

Acknowledgments

The authors are deeply grateful to Prof. Luigi Angiolini of the University of Bologna for helpful discussion.

This study was partially supported by the First TEAM grant No. POIR.04.04.00-00-5ED7/18-00, which is carried out within the First TEAM programme of the Foundation for Polish Science (FNP) co-financed by the European Union under the European Regional Development Fund.

Figure for TOC



Optical microscopy images of pristine PT6Br/F (left) and rrPT6Br/F (right).

References

- [1] O. Inganäs, *Adv. Mater.* **2018**, 1800388.
- [2] J. You, L. Dou, K. Yoshimura, T. Kato, K. Ohya, T. Moriarty, K. Emery, C. C. Chen, J. Gao, G. Li, *Nat. Commun.* **2013**, *4*, 1446.
- [3] K. Tvingstedt, O. Inganäs, *Adv. Mater.* **2007**, *19*, 2893.
- [4] P. A. Van Hal, J. Knol, B. M. W. Langeveld-Voss, S. C. J. Meskers, J. C. Hummelen, R. A. J. Janssen, *J. Phys. Chem. A* **2000**, *104*, 5974.
- [5] C. Y. Yang, A. J. Heeger, *Synth. Met.* **1996**, *83*, 85.
- [6] M. T. Dang, L. Hirsch, G. Wantz, *Adv. Mater.* **2011**, *23*, 3597.
- [7] G. A. Bernardin, N. A. Davies, C. E. Finlayson, *Materials Science in Semiconductor Processing* **2017**, *71*, 174.
- [8] K. Sivula, Z. T. Ball, N. Watanabe, J. M. J. Fréchet, *Adv. Mater* **2006**, *18*, 206.
- [9] G. T. Feng, J. Y. Li, F. J. M. Colberts, M. M. Li, J. Q. Zhang, F. Yang, Y. Z. Jin, F. L. Zhang, R. A. J. Janssen, C. Li, W. W. Li, *J. Am. Chem. Soc.* **2017**, *139*, 18647.
- [10] M. Chen, M. Li, H. Wang, S. Qu, X. Zhao, L. Xie, S. Yang, *Polym. Chem.* **2013**, *4*, 550.
- [11] J. U. Lee, A. Cirpan, T. Emrick, T. P. Russell, W. H. Jo, *J. Mater. Chem.* **2009**, *19*, 1483.
- [12] Y. Murata, M. Suzuki, K. Kamatsu, *Org. Biomol. Chem.* **2003**, *1*, 2624.
- [13] T. Yamazaki, Y. Murata, K. Komatsu, K. Furukawa, M. Morita, N. Maruyama, T. Yamao, S. Fujita, *Org. Lett.* **2004**, *6*, 4865.
- [14] M. Lanzi, L. Paganin, F. Errani, *Polymer*, **2012**, *53*, 2134.
- [15] R. C. Hiorns, E. Cloutet, E. Ibarboure, L. Vignau, N. Lemaitre, S. Guillerez, C. Absalon, H. Cramail, *Macromolecules* **2009**, *42*, 3549.
- [16] B. C. Thompson, J. M. J. Fréchet, *Angew. Chem. Int. Ed.* **2008**, *47*, 58.
- [17] B. J. Kim, Y. Miyamoto, B. Ma, J. M. J. Fréchet, *Adv. Funct. Mater.* **2009**, *19*, 2273.
- [18] M. H. Li, P. Xu, J. G. Yang, S. F. Yang, *J. Mater. Chem.* **2010**, *20*, 3953.
- [19] B. R. Panda, A. Chattopadhyay, *J. Nanosci. Nanotechnol.* **2007**, *7*, 1911.
- [20] A. Chou, K. C. Vernon, L. Piro, B. Radi, E. A. Jaatinen, T. J. Davis, *J. Phys. Chem. C* **2012**, *116*, 26517.
- [21] P. Costa Bizzarri, F. Andreani, C. Della Casa, M. Lanzi, E. Salatelli, *Synth. Met.* **1995**, *75*, 141.
- [22] M. Lanzi, L. Paganin, *Eur. Polym. J.* **2008**, *44*, 3987.
- [23] B. W. Bondouris, F. Molins, D. A. Blank, C. D. Frisbie, M. A. Hillmyer, *Macromolecules* **2009**, *42*, 4118.
- [24] R. Qian, *Makromol. Chem., Macromol. Symp.* **1990**, *33*, 327.
- [25] J. Clark, C. Silva, R. H. Friend, F. C. Spano, *Phys. Rev. Lett.* **2007**, *98*, 206406.
- [26] J. Clark, J. F. Chang, F. C. Spano, R. H. Friend, C. Silva, *Appl. Phys. Lett.* **2009**, *94*, 163306.
- [27] W. Barford, *J. Chem. Phys.* **2007**, *126*, 134905.
- [28] D. Beljonne, J. Cornil, R. Silbey, P. Millie, J. L. Brédas, *J. Chem. Phys.* **2000**, *112*, 4749.
- [29] S. Yamamoto, H. Yasuda, H. Ohkita, H. Benten, S. Ito, S. Miyanishi, K. Tajima, K. Hashimoto, *J. Phys. Chem. C* **2014**, *118*, 10584.
- [30] L. Echegoyen, L. E. Echegoyen, *Acc. Chem. Res.* **1998**, *31*, 593.
- [31] J. Pommerehne, H. Westweber, W. Guss, R. F. Mahrt, H. Bassler, M. Porsch, J. Daub, *Adv. Mater.* **1995**, *7*, 551.
- [32] T. V. Richter, C. H. Braun, S. Link, M. Scheuble, E. J. W. Crossland, F. Stelzl, U. Wuerfel, S. Ludwigs, *Macromolecules* **2012**, *45*, 5782.
- [33] M. C. Scharber, D. Muehlbacher, M. Koppe, P. Denk, C. Waldauf, A. J. Heeger, C. J. Brabec, *Adv. Mater.* **2006**, *18*, 789.
- [34] P. Schilinsky, C. Waldauf, J. Hauch, C. J. Brabec, *J. Appl. Phys.* **2004**, *95*, 2816.

- [35] W. B. Lai, C. Li, J. Q. Zhang, F. Yang, F. J. M. Colberts, B. Guo, Q. M. Wang, M. M. Li, A. D. Zhang, R. A. J. Janssen, M. J. Zhang, W. W. Li, *Chem. Mater.* **2017**, 29, 7073.
- [36] H. W. Tang, G. H. Lu, L. G. Li, J. Li, Y. Z. Wang, X. N. Yang, *J. Mater. Chem.* **2010**, 20, 683.
- [37] A. Lange, A. Hollaender, M. Wegener, *Materials Science and Engineering B* **2013**, 178, 299.
- [38] M. A. Ansari, S. Mohiuddin, F. Kandemirli, M. I. Malik, *RSC Adv.* **2018**, 8, 8319.
- [39] Y. Li, W. Huang, H. Huang, C. Hewitt, Y. Chen, G. Fang, D. L. Carroll, *Solar Energy* **2013**, 90, 51.
- [40] D. U. Karatay, M. Salvador, K. Yao, A. K. Y. Jen, D. S. Ginger, *Appl. Phys. Lett.* **2014**, 105, 033304.
- [41] L. Lu, Z. Luo, T. Xu, L. Yu, *Nano Lett.* **2013**, 13, 59.
- [42] F. Padinger, R. S. Rittberger, N. S. Sariciftci, *Adv. Funct. Mater.* **2003**, 13, 85.
- [43] V. D. Mihailetschi, H. Xie, B. de Boer, L. J. A. Koster, P. W. M. Blom, *Adv. Funct. Mater.* **2006**, 16, 699.
- [44] M. Drees, H. Hoppe, C. Winder, H. Neugebauer, N. S. Sariciftci, W. Schwinger, F. Schaffler, C. Topf, M. C. Scharber, Z. Zhu, R. Gaudiana, *J. Mater. Chem.* **2005**, 15, 5158.
- [45] Z. Zhu, S. Hadjikyriacou, D. Waller, R. Gaudiana, *J. Macromol. Sci. Part A* **2004**, 41, 1467.
- [46] K. S. Lee, K. Y. Yeon, K. H. Jung, S. K. Kim, *J. Phys. Chem. A* **2008**, 112, 9312.
- [47] Y. Tang, L. Ji, R. S. Zhu, Z. R. Wei, B. Zhang, *J. Phys. Chem. A* **2005**, 109, 11123.

Supplementary informations

Table 1 SI. Main IR absorption bands of homopolymers and copolymers

Assignment	PT6Br	rrPT6Br	PT6Br/F	rrPT6Br/F
ν C-H β thiophene	3055	3055	3053	3056
ν_{as} CH ₂	2929	2929	2929	2930
ν_{sym} CH ₂	2854	2854	2852	2852
ν_{as} C=C thiophene	1509	1505	1506	1513
ν_{as} C=C thiophene	1457	1432	1455	1456
fullerene	-	-	1429	1428
ν C-C thiophene-thiophene	1259	1258	1260	1259
fullerene	-	-	1182	1182
δ C-H thiophene	1090	1071	1034	1031
γ C-H thioph. 2,3,5-trisubstituted	827	826	834	836
γ C-H side chain	727	724	747	749
ν C-Br (aliphatic)	645, 562	642, 561	649, 560	646, 562
fullerene	-	-	576, 522	576, 525

ν = stretching; γ = out of plane bending; δ = in plane bending

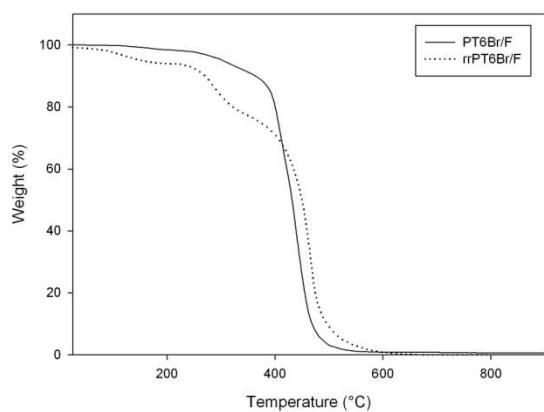


Figure 1 SI. TGA thermograms of copolymers.

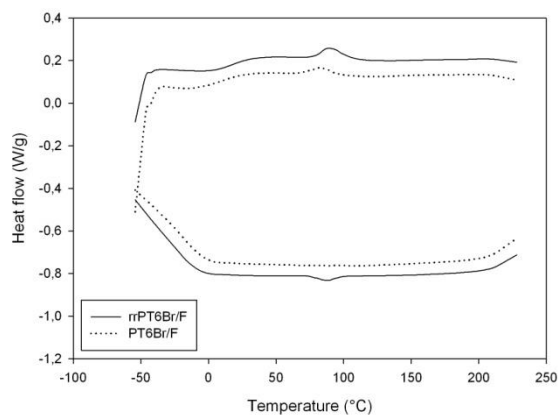


Figure 2 SI. DSC thermograms of copolymers (second scan).

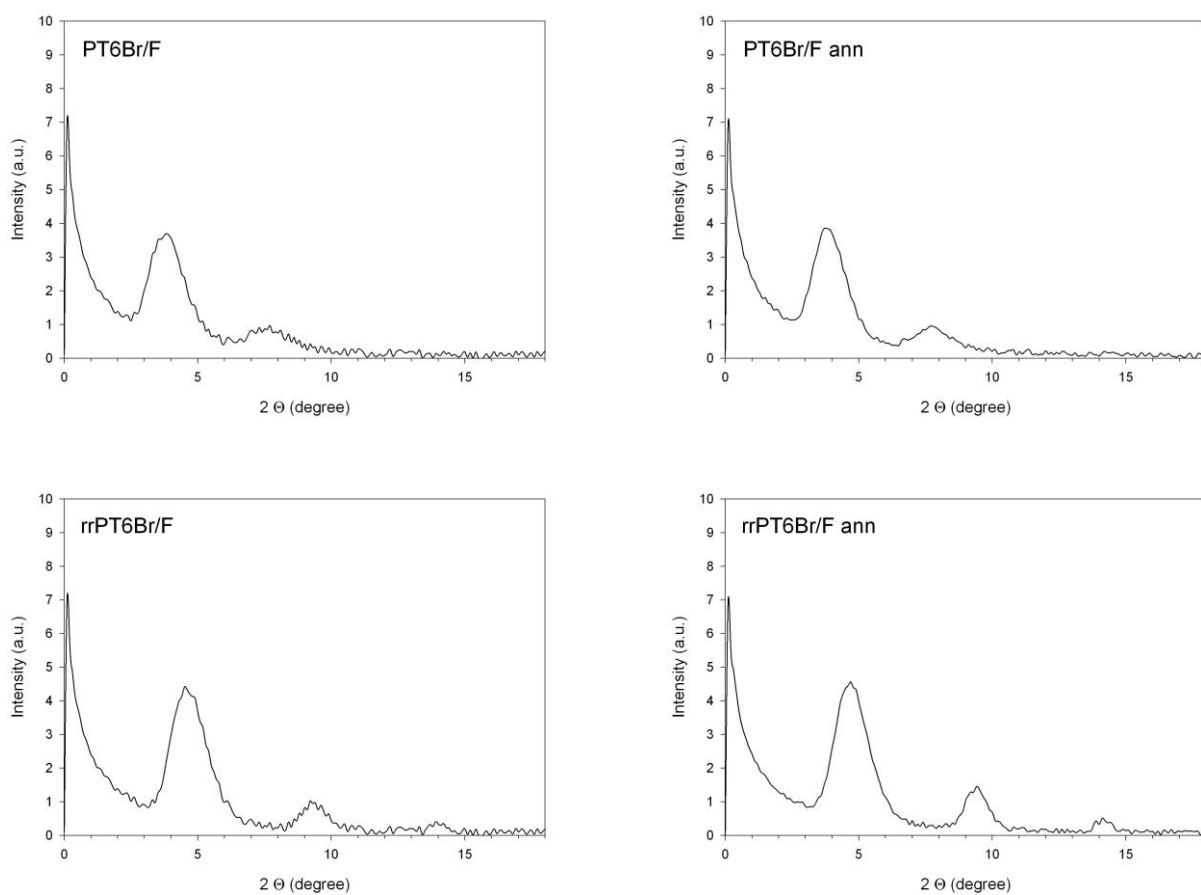


Figure 3 SI. X-rays diffractograms of copolymer films before (left) and after (right) the annealing procedure.

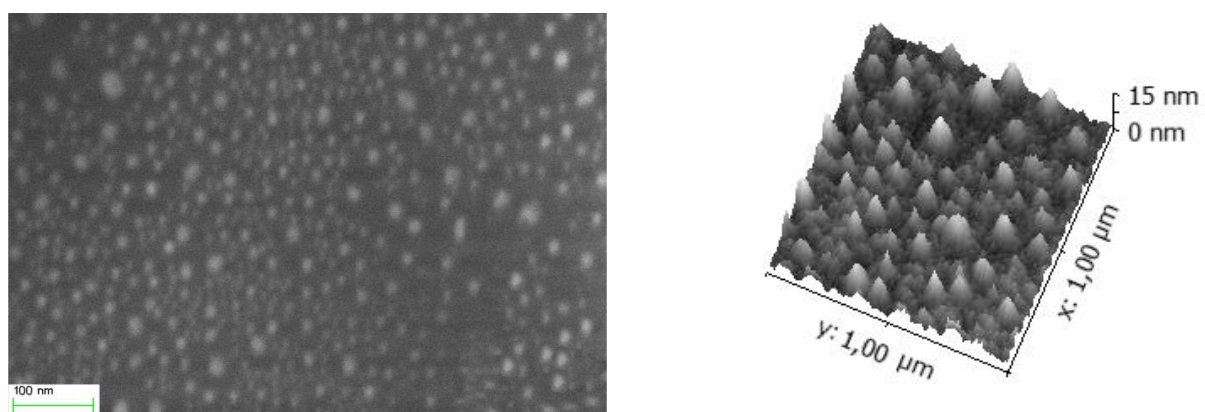


Figure 4 SI. SEM (left) and AFM (right) topography images of AuNPs layer.